A model-based analysis of foliar NOx deposition

Erin R. Delaria[1], Ronald C. Cohen[1,2]

[1]Department of Chemistry, University of California Berkeley, Berkeley, CA, USA
[2]Department of Earth and Planetary Science, University of California Berkeley, Berkeley, CA, USA

5   *Correspondence to*: Ronald C. Cohen (rccohen@berkeley.edu)

Abstract.

Foliar deposition of NO_2 removes a large fraction of the global soil-emitted NO_x. Understanding the mechanisms of NO_x foliar loss is important for constraining surface ozone, NO_x mixing ratios, and assessing the impacts of nitrogen inputs to ecosystems. We have constructed a 1D multi-box model with representations of chemistry and vertical transport to evaluate the impact of

10   leaf-level processes on canopy-scale concentrations, lifetimes, and canopy fluxes of NO_x. Our model is able to closely replicate canopy fluxes and above-canopy NO_x daytime mixing ratios observed during two field campaigns, one in a western Sierra Nevada pine forest (BEARPEX-2009) and the other a northern Michigan mixed hardwood forest (UMBS-2012). Our model demonstrates that NO_2 deposition can provide a mechanistic explanation for canopy reduction factors (CRFs). We show that foliar deposition can explain observations suggesting as much as ~60% of soil-emitted NO_x is removed within forest canopies.

15   Stomatal conductances greater than 0.1 cm s^{-1} result in modelled canopy reduction factors in the range of those used in global models, reconciling inferences of canopy NO_x reduction with leaf-level deposition processes. We also show that incorporating parameterizations for vapor pressure deficit and soil water potential has a substantial impact on predicted NO_2 deposition, with the percent of soil NO_x removed within one canopy increasing by ~15% in wet conditions compared to dry conditions. NO_2 foliar deposition was found to have a significant impact on ozone and nitrogen budgets under both high and low NO_x

20   conditions.

1 Introduction

The chemistry of nitrogen oxides ($NO_x \equiv NO + NO_2$) has a large impact on the oxidative capacity of the atmosphere and the budget of global surface ozone (Crutzen, 1979). NO_x is primarily removed from the atmosphere by chemical reactions to form nitric acid, alkyl nitrates, and peroxynitrates, and by dry deposition of NO_2 (Crutzen, 1979; Jacob and Wofsy, 1990; Romer et

25   al. 2016). The chemical loss pathways of NO_x have been extensively studied, but the physical loss to dry deposition remains much more uncertain. Globally, foliar deposition of NO_2 removes 20–50% of soil-emitted NO (Jacob and Wofsy,1990;Yienger and Levy, 1995), and constrains near-surface NO_x concentrations and input to ecosystems (Hardacre et al. 2015). Understanding the processes that control this removal of NO_x by the biosphere is important for predicting anthropogenic surface ozone and understanding flows in the nitrogen cycle.

Reactive nitrogen oxides also serve as an important nutrient in ecosystems. Exchange processes cycle nitrogen between the biosphere and atmosphere, influencing the availability of nitrogen to ecosystems (Townsend et al., 1996; Holland et al., 1997; Galloway et al., 2004; Holland et al., 2005). Deposition of atmospheric reactive nitrogen species can fertilize ecosystems with limited nitrogen availability (Ammann et al., 1995; Townsend et al., 1996; Williams et al., 1996; Holland et al., 1997; Galloway et al., 2004; Teklemariam and Sparks, 2006). Although nitrogen is often the limiting nutrient for plant growth (Oren et al., 2001; Galloway et al., 2004), anthropogenic activities have in some cases caused an excess loading of nitrogen to ecosystems, leading to dehydration, chlorosis, soil acidification, and a decline in productivity (Vitousek et al.,1997; Fenn et al., 1998; Galloway et al., 2004).

The current understanding of the exchange of nitrogen oxides between the atmosphere and biosphere remains incomplete. Despite the importance of dry deposition processes, they are among the most uncertain and poorly constrained aspects of atmosphere-biosphere nitrogen exchange and the tropospheric budgets of O_3 and NO_x (Wild, 2007; Min et al., 2014; Hardacre et al., 2015). This uncertainty arises from the complex dependence of dry deposition processes on surface cover, meteorology, seasonal changes in leaf area index (LAI), species of vegetation, and the chemical species carrying odd-N. Developing a mechanistic understanding of dry deposition of NO_x has largely depended on inferences from scarce long-term field observation data and a limited number of laboratory studies on the effects of environmental factors on deposition at the leaf-level. This understanding is represented by a deposition velocity, V_d.

The deposition velocity of NO_2 to vegetation is largely regulated by stomatal conductance (Johansson, 1987; Thoene et al., 1991; Rondon and Granat, 1994; Teklemariam and Sparks, 2006; Chaparro-Suarez et al., 2011; Breuninger et al., 2012; Delaria et al., 2018), which varies with tree species, photosynthetically active radiation (PAR), vapour pressure deficit (VPD), temperature (T), soil water potential (SWP) and season (Emberson et al., 2000; Altimir et al., 2004; Hardacre et al., 2015; Kavassalis and Murphy, 2017). Many global scale chemistry transport models (Jacob and Wofsy, 1990; Wang and Leuning, 1998; Ganzeveld et al., 2002) parameterize V_d using the resistance in-series approach similar to that developed by Wesely (1989). These treatments are heavily parameterized, leading to a large degree of uncertainty, and do not account for the effects of VPD, SWP, CO_2 mixing ratio, or other factors known to influence stomatal conductance (Hardacre et al., 2015). NO_x deposition remains even more uncertain than deposition of O_3, where stomatal response has been shown to be the primary regulator of foliar deposition and mesophyllic resistance to deposition is negligible. Observations from leaf-level laboratory studies suggest mesophyllic resistance is important for controlling the deposition velocity of NO_2 (Chaparro-Suarez et al., 2011; Breuninger et al., 2012). A failure to consider the effects of relevant meteorology on stomatal conductance, as well as our deficient understanding of mesophyllic resistances and the diversity of ecosystem responses, severely limits our ability to understand dry-deposition processes and how they will be affected by feedbacks from changes in climate, land use, and air pollution.

The importance of these considerations has recently been illustrated by Kavassalis and Murphy (2017), who found a significant correlation between VPD and ozone loss, and demonstrated that modeling using VPD-dependent parameterizations of deposition better predicted the correlation they observed. Previous work by Altimir el al. (2004) and Gunderson et al. (2002)

have described the effects of VPD and other environmental parameters on the stomatal conductance to O$_3$ of *Pinus sylvestris* and *Liquidambar styraciflua*, respectively. More recent models, like the DO3SE model for estimating ozone fluxes and damage to plants, incorporate the effects of VPD an SWP on stomatal conductance, but no similar model exists for assessing these effects on NO$_x$ deposition. The DO3SE has successfully been implemented in the European Monitoring and Evaluation

5 Program (EMEP) regional model (2012). Modelling studies by Buker et al. (2007) and Emberson et al. (2000) have also demonstrated the success of regional-scale parameterizations using observed relationships between meteorology and stomatal conductance for application to O$_3$.

In this study we present a multi-layer atmosphere-biosphere exchange model and investigate the sensitivity of NO$_x$ canopy fluxes, ozone production, NO$_x$ vertical profiles, and NO$_x$ lifetimes to different parameterizations of stomatal

10 conductance, leaf area index, and deposition velocity. There have been many studies investigating the effects of dry-deposition parameterizations on deposition velocities—particularly of ozone—and the abilities of different modeling schemes to reproduce observational data for other molecules (Zhang et al., 1996; Wang and Leuning, 1998; Wang et al., 1998b; Emberson et al., 2000; Ganzeveld 2002; Buker et al., 2007; Wolfe et al., 2011; Hardacre et al., 2015; Nguyen et al., 2015). However, there has been little evaluation of how changes in dry deposition of NO$_2$ may affect surface mixing ratios and chemistry of

15 important atmospheric species. Assessing the sensitivity to NO$_2$ deposition is crucial not only for evaluating the potential impact of the uncertainties of dry-deposition parameterizations for global and regional models, but for understanding how a changing climate may influence NO$_x$, surface ozone, and the nitrogen cycle.

2 Model description

We have constructed a detailed atmospheric model for investigating the influence of leaf-level NO$_x$ foliar deposition on canopy

20 scale NO$_x$ lifetimes and concentrations. The model consists of eight vertical boxes below the boundary layer (PBL), taken to be 1000 m during the day and 60 m at night. The increase in PBL height during the day is treated as a gaussian function of time with 98% of the integrated area contained between sunrise and sunset, with the maximum height reached at the time of maximum daily temperature (Fig.1).

In each box, the change in concentration (C) of species i, is calculated using the time-dependent continuity equation:

25 $$\frac{\partial C_i(z)}{\partial t} = P(z) + L(z) + E(z) + D(z) + A(z) + \frac{\partial F(z)}{\partial z} \qquad (1)$$

where the terms on the right are the chemical production, chemical loss, emission, deposition, advection, and turbulent flux, respectively. In each box (k=1–8) the altitude (z) is considered as the average of the altitudes at the upper boundaries of boxes k and $k-1$. The change in concentration for species i is calculated for each time step $\Delta t = 2$ s.

$$\Delta C_{i,k} = \left(P_{i,k} + L_{i,k} + E_{i,k} + D_{i,k} + A_{i,k} + \frac{F_{i,k}}{\Delta h_k} \right) \Delta t \qquad (2)$$

30 where Δh_k is the width of box k. The only species not treated in this manner is the hydroxyl radical (OH), which is calculated using a steady-state approximation.

The model is evaluated by comparison to observations from the Biosphere Effects on Aerosols and Photochemistry 2009 (BEARPEX-2009) field campaign from 15 June – 31 July 2009 (Min et al., 2014), and the University of Michigan Biological Station (UMBS) during 5 August – 10 August 2012 (Geddes and Murphy, 2014). For the BEARPEX-2009 calculations, the modelled canopy included an overstory height of 10 m with a one-sided leaf area index (LAI) of 3.2 m^2m^{-2}

5   (LAI_{os}), and an understory height of 2 m with a LAI of 1.9 m^2m^{-2} (LAI_{us}). Model simulations were run for June 30, 2009 using conditions from the BEARPEX-2009 ponderosa pine forest site located in the western foothills of the Sierra Nevada Mountains, CA (38°58'42.9"N, 120°57'57.9"W, elevation 1315 m) (Table 1) (Fig. 2a). For UMBS-2012 calculations, the modelled canopy included an overstory height of 20 m with a total one-sided LAI of 3.5 m^2m^{-2}. Model simulations were run for August 8, 2012 using conditions from the UMBS mixed hardwood forest located in northern Michigan (45°33'32" N,

10   84°42'52" W) (Table 1) (Fig 2b). In the BEARPEX-2009 case, meteorological conditions and soil NO_x emissions used in the model simulation were those reported in Min et al. (2014). Diurnal soil water potentials (SWP) were values reported in a geological survey of nearby Sierra sites and a comparatively wet year (Ishikawa and Bledsoe, 2000; Stern et al., 2018). For the UMBS-2012 case, daily temperatures, VPDs, soil NO_x emissions and site-specific parameters used in the model simulations were those reported in Geddes and Murphy (2014), and Seok et al. (2013). Temperature and relative humidity

15   used in the model were sinusoidal fits to observations of minimum and maximum daily temperature and relative humidity from the corresponding field measurement site. The relative temperature decrease as a function of altitude was calculated using a fit to observations during BEARPEX-2007, as presented by Wolfe and Thornton (2011). Solar zenith angles (SZA) and photosynthetically active radiation (PAR) were calculated every 0.5 h for each location and time period using the National Center for Atmospheric Research TUV calculator (Madronich and Flocke, 1999) and fit using a smoothed spline interpolation.

20   Within the canopy, extinction of radiation (ER) was calculated as:

$$ER_k = \exp\left(-\frac{k_{rad}LAI_{cum}}{\cos(SZA)}\right) \tag{3}$$

where k_{rad} is the radiation extinction coefficient, SZA is the solar zenith angle, and LAI_{cum} is the cumulative LAI calculated as the sum of one-half the LAI in box k and the total LAI in the boxes above box k.

25   **2.1 Vertical transport and advection**

Turbulent diffusion ($F(z)$) is represented in the model using K-theory:

$$F(z) = -K(z)\frac{\Delta C_{i,k}}{\Delta z} \tag{4}$$

where $\Delta C_{i,k}$ is the change of concentration in species i in box k during each timestep and Δz is the difference between the midpoints of boxes k and $k+1$. $K(z)$ above the canopy is based on the values from Gao et al. (1993) and below is a function

30   of friction velocity calculated according to Wolfe et al. (2011) and is a function of the diffusion timescale ratio (τ/T_L) and the friction velocity (u^*). The resulting residence time in the canopy is approximately 2 min for model conditions.

Advection in the model is treated as a simple mixing process in each model layer.

$$\left(\frac{dC_i}{dt}\right) = -k_{mix}\left(C_i - C_{i(adv)}\right) \tag{5}$$

where $k_{mix} = 0.3$ h^{-1} (Wolfe and Thornton, 2011), and $C_{i(adv)}$ is the advection concentration of species i. Advection concentrations are set to fit with the observations during BEARPEX-2009 (Min et al., 2014) or UMBS-2012 (Geddes and Murphy, 2014; Seok et al., 2013) and are used to maintain reasonable concentrations (Table S1). For the BEARPEX-2009

5   model runs, the maximum daily advection concentration was reached at around 17 hrs, based on field observations of higher NO$_x$ plumes from near-by Sacramento in the afternoon (Wolfe et al., 2011; Min et al., 2014).

2.2 Chemistry

Chemistry in the model is based on reaction rate constants from the JPL Chemical Kinetics and Photochemical Data Evaluation No. 18 (Burkholder et al., 2015). Photolysis rates are calculated as a function of solar zenith angle (SZA), which
10   was constructed using a smoothed spline interpolation fit of photolysis rates calculated with the TUV calculator (Madronich and Flocke, 1999) at every ten-degree interval of the zenith angle. The simplified reaction scheme included in the model is based on the model presented in Browne and Cohen (2012). The model includes both daytime and night-time NO$_x$ chemistry and a simplified oxidation scheme. In this simplified case, oxidation of volatile organic compounds (VOCs) during the daytime results in the production of peroxy radicals (RO$_2$), treated as a uniform chemical family. To be applicable to a range of forest
15   types, we also include adjustable parameters, *kOH* and *kNO$_3$* for the average site-specific rate constant for reaction of VOC with OH and NO$_3$. A complete list of reactions and rate constants included in the model is shown in Table S2.

2.3 Emission and deposition

Emissions rates (molecules cm^{-3}s^{-1}) of biogenic volatile organic compounds (BVOCs) in the canopy are calculated via:

20   $$E(z) = \frac{E_b}{\Delta h}C_L(z)C_T(z)LAI \tag{6}$$

where E_b (molecules cm(leaf)$^{-2}$ s^{-1}) is the basal emission rate of VOC, Δh is the total height of the box, and C_L and C_T are corrections for light and temperature (Guenther et al., 1995). The deposition flux (F_{dep}) of each depositing species i in the canopy is calculated according to:

$$F_{dep} = -V_d \cdot LAI \cdot C_i \tag{7}$$

25   where LAI is the leaf area index, and V_d is the deposition velocity. The deposition velocities are calculated according to:

$$V_d = \frac{1}{R} \tag{8}$$

where R is the total resistance to deposition.

$$R_{leaf} = \left(\frac{1}{R_{cut}} + \frac{1}{R_{st}+R_m}\right)^{-1} \tag{9}$$

$$R = R_a + R_b + R_{leaf} \tag{10}$$

where R_a, R_b, R_{cut}, R_{st}, and R_m are the aerodynamic, boundary layer, cuticular, stomatal, and mesophilic resistances, respectively. These resistances describe the turbulent transport of a gas to the surface (R_a), molecular transport of through a thin layer of air above the leaf surface (R_b), and deposition to the leaf surface (R_{leaf}) (Baldocchi et al., 1987). R_{leaf} is dependent upon plant physiology and determined by deposition to the leaf cuticles (R_{cut}), diffusion through the stomata (R_{st}), and

5   chemical processing within the mesophyll (R_m). We do not include compensation points in our parameterization of NOx dry deposition, in accordance with numerous recent studies that have observed no evidence of NO2 emission at low NOx mixing ratios (Chaparro-Suarez et al., 2011; Breuninger et al., 2013; Delaria et al., 2018)

All boundary, aerodynamic, cuticular, and soil resistances of O3, HNO3, CH2O, alkyl nitrates (ANs) and peroxyacyl nitrates (APNs), HC(O)OH, ROOH, and H2O2 are calculated according to Wolfe et al. (2011). The cuticular and mesophylic

10 resistances for NO2 and NO are adjustable input parameters. Stomatal resistances are determined from the stomatal conductance to water vapor (g_s) calculated using either Eq. 11 (Wesely, 1989), or Eq. 12 (Emberson et al., 2000), hereafter referred to as the Wesely and Emberson schemes, respectively:

$$g_s = g_{max} \times \frac{T(40-T)/400}{(1+(200(SR+0.1)^{-1})^2} \tag{11}$$

$$g_s = g_{max} \times f_{phen} \times f_{light}\max\{f_{min}, (f_{temp} \times f_{VPD} \times f_{SWP})\} \tag{12}$$

15 where g_{max} is the species specific maximum stomatal conductance, f_{min} is a species-specific scaling factor to the minimum stomatal conductance, and f_{phen}, f_{SWP}, f_{light}, f_{temp}, and f_{VPD} are functions representing modifications to the stomatal conductance due to leaf phenology, soil water content, irradiance, temperature, and vapor pressure deficit, respectively (Eq 13–16).

$$f_{light} = 1 - \exp(-Light_a \times PPFD) \tag{13}$$

20 $$f_{temp} = 1 - \frac{(T-T_{opt})^2}{(T_{opt}-T_{min})^2} \tag{14}$$

$$f_{VPD} = \min\{1, \left((1-f_{min}) \times \frac{(VPD_{min}-VPD)}{(VPD_{min}-VPD_{max})}\right) + f_{min} \tag{15}$$

$$f_{SWP} = \min\{1, \left((1-f_{min}) \times \frac{(SWP_{min}-SWP)}{(SWP_{min}-SWP_{max})}\right) + f_{min} \tag{16}$$

T_{opt} and T_{min} are the optimal and minimum temperature required for stomatal opening. PPFD is the photosynthetic photon

25 flux density and $Light_a$ is a species-specific light response parameter. VPD_{min} and VPD_{max} are the vapor pressure deficit at which stomatal opening reaches a minimum and maximum, respectively. SWP_{min} and SWP_{max} are the soil water potentials at which stomatal opening reaches a minimum and maximum, respectively. All model calculations represented the peak growing season when $f_{phen}= 1$. f_{temp}, f_{VPD}, and f_{light} were calculated according to Emberson et al. (2000) using parameters found in Table 2.

2.4 Evaluation of NO$_x$ fluxes and lifetimes

The model was used to assess the impact of NO$_x$ deposition parameters on the NO$_x$ budget, lifetimes, loss, and vertical profiles within a forested environment. In each box, the rates of NO$_x$ loss with respect to nitric acid formation, alkyl nitrate formation, and deposition were calculated from Eq. 17–19.

$$L_{NO_x \to HNO_3} = k_{OH+NO_2}[OH][NO_2] + k_{N_2O_5\ hydrolosis}[N_2O_5] + k_{NO_3+aldehyde}[\text{aldehyde}][NO_3] \tag{17}$$

$$L_{NO_x \to RONO_2} = \alpha k_{NO+RO_2}[NO][RO_2] + \beta k_{NO_3}[NO_3][VOC] \tag{18}$$

$$L_{NO_x \to Dep} = F_{dep}/\Delta h_k \,, \tag{19}$$

α is the fraction of the NO + RO$_2$ reaction that forms alkyl nitrates and β is the fraction of the NO$_3$ + BVOC reaction that forms alkyl nitrate. The NO$_x$ lifetime was then scaled to the entire boundary layer by summing over the products of the lifetime and boundary layer fraction ($\Delta h_k/PBL$) in each box

$$\tau_{PBL} = \frac{\sum_{k=1}^{8}[NO_x]_k}{\sum_{k=1}^{8}(L_{NO_x \to Dep}+L_{NO_x \to RONO2}+L_{NO_x \to HNO3})} \tag{20}$$

NO$_x$ was treated as the sum of NO, NO$_2$, and all short-lived products, including NO$_3$, 2N$_2$O$_5$, and, during the daytime, peroxyacetyl nitrate (PAN). During the nighttime PAN has a longer atmospheric lifetime (>10 h) and was treated as a permanent sink (Romer et al., 2016). Lifetime against PAN formation at night was calculated from:

$$L_{NO_x \to PAN} = k_{NO_2+acetylperoxy}[NO_2][CH_3C(O)O_2] \tag{21}$$

We also calculated the 24 h average vertical fluxes of NO$_x$, and used the flux through the canopy to estimate the fraction of soil emitted NO$_x$ ventilated to the troposphere above. Because PAN formed during nighttime is expected to re-release NO$_x$ to the atmosphere during the day, in this calculation, PAN was included as part of the NO$_x$ budget.

3 Sensitivity to parameterizations

We assessed the sensitivity of the model to τ/T_L, the radiation extinction coefficient (k_{rad}), the aerodynamic leaf width (l_w), LAI, soil NO emission (eNO), and α. These parameters are simplifications of complex physical processes and not always easily constrained by observations. The total deposition velocity of NO$_x$ chosen for these assessments was 0.2 cm s^{-1} during the daytime and 0.02 cm s^{-1} during the night-time.

The largest effects were observed for changes in α, LAI, and soil NO emission. LAI$_{os}$ and LAI$_{us}$ were scaled from their values of 1.9 m^2/m^2 and 3.2 m^2/m^2, respectively by a factor of 0.25 and 1.5. Increasing the scaling factor from 0.25 to 1.5 results in a decrease of NO$_x$ lifetimes, above canopy concentration, and average canopy flux of 24%, 27%, and 36%, respectively (Fig. S1). Increasing α from 0.01 to 0.1 results in a decrease in NO$_x$ lifetimes, above canopy concentration, and average canopy flux of 75%, 38%, and 39%, respectively (Fig. S2). For all other model runs an α of 0.075 was chosen, in accordance with observations from regions primarily influenced by BVOCs (eg. monoterpenes, isoprene, 2-methyl-3-buten-2-ol). Increasing the maximum soil NO emission from 1 to 10 ppt m s^{-1} increased the in-canopy enhancement from 28% to 140% relative to above-canopy NO$_x$ concentrations (Fig. S3b). The fraction of soil-emitted NO$_x$ ventilated through the canopy

also increased from 45% to 64% (Fig. S3a). The large effect of soil NO emission on NO_x fluxes implies that this highly variable parameter (Vinken et al., 2014) is also important to constrain in chemical transport models. Further discussion of soil NO emission is, however, beyond the scope of this study.

Very small effects on NO_x were observed for changes in the parameters τ/T_L, k_{rad}, or l_w. The minor changes caused by variations in these parameters are listed below for completeness:

τ/T_L represents the diffusion timescale ratio, a full description of which can be found in Wolfe and Thornton (2011). Large τ/T_L represents faster diffusion and vertical transport within the canopy layer, and shorter residence times in the canopy. We find that altering this parameter from 1.2 to 8 (representing a change in residence time from 650 s to 62 s) causes a 9.9%, 4.4%, and 8.7% increase in average canopy fluxes, NO_x lifetimes and above canopy concentration, respectively (Fig. S4). For all subsequent model runs, a value of 2 for τ/T_L was chosen, resulting in a canopy residence time of 152 s, calculated using Eq.22.

$$\tau_{can} = h_{can} \sum_{k=1}^{3} \frac{\Delta h_k}{K(z_k)} \tag{22}$$

This residence time is consistent with observations of a variety of forest environments (Jacob and Wofsy, 1990; Wolfe et al., 2011).

The boundary layer resistance, or laminar sublayer resistance, R_b, is dependent upon the aerodynamic leaf width, l_w (Eq.23)

$$R_b = \frac{cv}{Du^*(z)} \left(\frac{l_w u^*(z)}{v} \right)^{1/2} \tag{23}$$

where $v = 0.146$ cm^{2}s^{-1} is the kinematic viscosity of air, D is the species-dependent molecular diffusion coefficient, c is a tuneable constant set to 1 for this study, and $u^*(z)$ is the height-dependent friction velocity that is a function of u^* and LAI_{cum} (Wolfe and Thornton, 2011). l_w depends upon the vegetation species. A value of 1 cm was chosen for the overstory and 2 cm for the understory, as these widths are characteristic of pine trees and understory shrubs in a poderosa pine forest (Wolfe and Thornton, 2011). Species with rapid deposition to the cuticles or the stomata are expected to be more sensitive to errors in l_w, such as HNO_3 or H_2O_2. An increase in NO_x lifetime, average canopy flux, and above canopy concentration of 1.4%, 2.4%, and 2.8%, respectively, is predicted for a change in l_w scaling factor from 0.1 to 2 (Fig. S5). These changes are expected to be greater in forests with a larger average deposition velocity.

The rates of stomatal gas exchange and photolysis are regulated by the intensity of light that penetrates the canopy. The extinction of radiation by the canopy, treated as a Beer's Law parameterization (Eq. 3) is exponentially proportional to the radiation extinction coefficient, k_{rad}. k_{rad} ranging from 0.4–0.65 has been measured for coniferous forests and understory shrubs (Wolfe and Thornton, 2011). The NO_x lifetime increases by 2.7% and the canopy fluxes, and above-canopy concentrations decrease by 0.7% and 0.6%, respectively, for a change in k_{rad} from 0 to 0.6 (Fig. S6). This effect is expected to be greater for forests with larger LAI. The minimal effect of k_{rad} on model results is was also observed for multiple canopy profile shapes of equivalent LAI.

4 Results

4.1 Model validation: comparison to observations

To evaluate the applicability of our 1D multilayer canopy model for predicting NO_x concentrations and vertical fluxes in a variety of forest environments, we compared the model to observations from BEARPEX-2009 and UMBS-2012. Parameters

5 used in each calculation are shown in Table 1. The model was run using both the Emberson and Wesely stomatal conductance models. Parameters for temperature, drought stress, and maximum and minimum stomatal conductances used in the Emberson model were input for the dominant tree species in the region (Table 2). At the BEARPEX-2009 site, the dominant tree species was ponderosa pine. For this site, g_{max} and parameters for f_{SWP} and f_{VPD} were inferred from ponderosa pine stomatal conductance data (Kelliher et al., 1995; Ryan et al., 2000; Hubbard et al., 2001; Johnson et al., 2009; Anderegg et al., 2017),

10 and f_{light} was inferred from measurements of the canopy conductance during BEARPEX-2009 (Fig 3a). f_{temp} was represented by observations for Scots pine (Altimir et al., 2004; Emberson et al., 1997; Buker et al., 2012) and validated with comparison to stomatal conductance measured via sap-flow during BEARPEX-2009 (Fig 3a). At UMBS the dominant species are quaking aspen and bigtooth aspen, with many birch, beech, and maple species also present (Seok et al., 2013). Data for a European beech tree species was used to represent stomatal conductance parameters (Buker et al., 2007; Buker et al., 2012)

15 and SWP stress (Emberson et al., 2000). These parameters were validated with comparison to stomatal conductance calculated from water vapor and latent heat flux measurements during UMBS-2012 using an energy-balance method according to Mallick et al. (2013) (Fig 4a).

The model replicates key features of the canopy fluxes and above-canopy NO_x daytime mixing ratios from the 2009 BEARPEX campaign (Fig.3). The average daytime above-canopy NO_x mixing ratios during the duration of BEARPEX-2009

20 were 253 ppt, with observations ranging from 80–550 ppt of NO_2 and 10–100 ppt of NO (Min et al., 2014). The general daily trends in observations of NO_x mixing ratios are captured by both the Wesely and Emberson cases—with minimum NO_x mixing ratios occurring in the late morning, an increase of NO_x in the afternoon, and maximum NO_x concentrations of 450–500 ppt reached in the evenings, primarily as a result of high-NO_x plumes from near-by Sacramento in the afternoon (Wolfe et al., 2011; Min et al., 2014). However, both model scenarios predict a slower than observed decrease in NO_x mixing ratios from

25 the evening to the early morning, larger midday fluxes than observed, and fail to represent the in-canopy enhancement of NO_x observed in the evening. The above-canopy vertical NO_x flux predicted in both model cases also agrees reasonably well with observations, with the Emberson case representing morning and midday NO_x fluxes slightly better than the Wesely case. This relatively good agreement between the Emberson case and observed fluxes is also demonstrated in Fig 3d by the agreement between modelled and observed canopy NO_x enhancements. There is, however, generally little difference between Emberson

30 and Wesely model cases for this site during the period considered (Fig 3). This is likely due to the good agreement in both the Emberson and Wesely cases to observations of stomatal conductance (Fig 3a).

We also observe similar correspondence between the model and key features of the UMBS-2012 observations (Fig 4). NO and NO_2 mixing ratios and canopy fluxes are both within the range of observations. The model predicts slightly lower

NO$_2$ in the morning and higher NO$_2$ at night than what was observed. Differences between the Wesely model and Emberson model were negligible for this site. This is likely due to a higher humidity in the summer in this region and larger soil moisture, reducing the prediction for midday and late afternoon VPD stress by the Emberson model, as can be seen by the similarity in the predicted g$_s$ by the Emberson and Wesely models (Fig 4a).

5   4.2 Effects of maximum stomatal conductance

The BEARPEX-2009 case was simulated using the Weesly model for different values of g_{max} (Fig 5). The range of g_{max} currently represented in the literature during peak growing season for forested regions ranges from 0.2–0.8 cm s^{-1} (Kelliher et al., 1995; Emberson et al., 1997; Emberson et al., 2000; Ryan et al., 2000; Hubbard et al., 2001; Altimir et al., 2003; Fares et al., 2013). This range reflects differences in forest types and a wide variety of tree species. Global CTMs using
10   the Wesely parameterization currently include g_{max} of 1.4, 0.77, and 1 cm s^{-1} for deciduous, coniferous, and mixed forests, respectively (Wesely, 1989; Wang et al., 1998a). Figure 5b demonstrates the impact of total leaf resistance on the average daily vertical flux of NO$_x$ through the canopy. 96% of soil emitted NO$_x$ is ventilated through the canopy with no foliar deposition (g_{max}= 0 cm s^{-1}). In contrast, 44% of soil-emitted NO$_x$ is taken up by the forest and 56% ventilated through the canopy when the maximum stomatal conductance (g_{max}) is 1.4 cm s^{-1}. Figures 5c and 5d show the effects of g_{max} on the
15   diurnal flux through the canopy and the diurnal above canopy NO$_x$ mixing ratio, respectively. Compared with no foliar deposition, a g_{max} of 1.4 cm s^{-1} results in ~60% reduction in the canopy flux and ~50% reduction in the above-canopy NO$_x$ mixing ratio at noon. (Fig. 5c, d). In Figure 6a we show the fraction of soil-emitted NO$_x$ ventilated through the canopy as a function of g_{max}. The model suggests a maximum foliar reduction of NO$_x$ of ~60% for a canopy of 10 m and total LAI of 5.1 m^2/m^2. Our model also predicts that changes in g_{max} have a greater overall impact on canopy NO$_x$ fluxes at larger leaf
20   resistances and slower foliar uptake. In the range for g_{max} of ~0–0.5 cm s^{-1}, variation in g_{max} can have a large impact on the predicted canopy fluxes of NO$_x$, which would in turn have large impact on concentrations and fluxes of O$_3$. This range of deposition velocities is the range expected for most forests, based on laboratory measurements of leaf-level deposition (Hanson and Lindberg, 1991; Rondon and Granat, 1994; Hereid and Monson, 2001; Teklemariam and Sparks, 2006; Pape et al., 2008; Chaparro-Suarez et al., 2011; Breuninger et al., 2013; Delaria et al., 2018) and global analysis suggesting 20–50% reductions
25   in soil-emitted NO$_x$ by vegetation (Jacob and Wofsy, 1990; Yienger and Levy, 1995). Model calculations also predict a strong effect on the lifetimes of NO$_x$, as shown in Figure 6b, with a deposition velocity of 0.3 cm s^{-1} reducing the NO$_x$ lifetime by ~1.8 hrs (~18%) and a deposition velocity of 1.4 cm s^{-1} reducing the NO$_x$ lifetime by ~3.6 hrs (~36%) compared with no deposition.

4.3 Emberson model vs. Wesely model comparison

30   As was demonstrated in our comparison of the model to observations from BEARPEX-2009 and UMBS-2012, the relative importance of including parameterizations of VPD and SWP in the calculation of stomatal conductance and overall deposition

velocity is regionally variable. We ran the model using BEARPEX-2009 conditions using both the Wesely and Emberson stomatal conductance models under "dry" and "wet" conditions. Under the "dry" scenario the SWP daily minimum and maximum were of -2.0 MPa and -1.7 MPa, respectively, with the daily minimum reached at sunset. A minimum daily RH of 40% occurred at noon, with a maximum at midnight of 65%. Summertime is often even drier in regions of the western United

5   States, so these "dry" parameters are conservative estimates for many forests. Under the "wet" scenario the SWP daily minimum and maximum were -0.5 MPa and -0.1 MPa, respectively. The maximum and minimum RH were 90% and 80%, respectively.

The results of the Wesely and Emberson "wet" and "dry" model runs are shown in Figure 8. There was only a slight decrease of the in-canopy NO_x enhancement and of the canopy fluxes in the Wesely "wet" case, presumably due to a slight

10 increase in OH radicals at higher RH. Predictably, the difference in the modelled deposition velocities was quite dramatic between the Emberson "wet" and "dry" cases. In the "dry" scenario, the deposition velocity reached a maximum in the late morning, but rapidly declined to a minimum shortly after noon. The maximum deposition velocity reached was also substantially reduced (Fig 7a). Using the "wet" Emberson stomatal conductance model, the NO_x flux out of the forest was reduced by 16% midday compared to the "dry" case, and the percent of soil NO_x removed within the canopy was increased

15 from 18% to 30% (Fig 7). The model calculates a substantial impact on above-canopy NO_x mixing ratios (Fig. 8), with a maximum of ~30% difference in NO_x in the afternoon between "wet" and "dry" days using the Emberson parameterizations, compared with ~10% difference using the Wesely model. Using the Emberson parameterization of stomatal conductance, deposition during "wet" days is predicted to contribute substantially more to the total NO_x loss (~40%), with only ~15% contribution is predicted for "dry" days (Fig. 9).

20   Under the Wesely model, where stomatal conductance is parameterized only with temperature and solar radiation, the predicted deposition velocity would be nearly identical between the spring and fall in the western United States and similar semi-arid regions (with comparatively minor temperature effects). The Emberson model predicts large seasonal differences. The Wesely model fails to account for the dramatic decrease in stomatal conductance seen in the dry seasons in such regions caused by significant reductions in relative humidity and soil water potential (Prior et al., 1997; Panek and Goldstein, 2001;

25 Chaves, 2002; Beedlow et al., 2013).

5 Discussion

5.1 Implications for modelling NO_2 dry deposition

As in our multilayer canopy model, the most common current method of parameterizing stomatal and cuticular deposition in large-scale chemical transport models (CTMs) is through the resistance model framework of Baldocchi (1987).

30 Many global (e.g. WRF-Chem and GEOS-Chem) and regional (e. g. MOZART and CAMx) CTMs calculate the stomatal component of the total deposition resistance using the representation of Wesely (1989), where stomatal conductance is dependent only on the type of vegetation, temperature, and solar radiation. The limitations of this parameterization have been

highlighted by observations of a strong dependence of foliar deposition on soil moisture and vapor pressure deficit (VPD) (Kavassalis and Murphy, 2017; Rydsaa et al., 2016). Inadequate descriptions of vegetative species, soil moisture, drought stress, etc., can have a dramatic impact on model results, and result in significant discrepancies between models and observations (Wesely and Hicks, 2000). Failure to account for effects of plant physiology on deposition may result in

5   misrepresentation of deposition velocities, which, as we demonstrate, can have a substantial impact on NO_x lifetimes and mixing ratios above and within a forest canopy. This effect will be especially pronounced in areas, such as much of the western United States, where there are frequent periods of prolonged drought. Parameterizations of stomatal conductance, such as those presented in Emberson et al. (2000) and incorporated into some regional-scale CTMs (e.g. EMEP, MSC-W, and CHIMERE), if incorporated into global atmospheric models, could more accurately reflect the dependence of foliar deposition on

10 meteorology and soil conditions. However, additional laboratory and field measurements on diverse plant species are also needed to determine appropriate, ecosystem-specific inputs to these parameterizations.

It should be noted that there have been significant recent advances in optimization approaches of stomatal modelling based on the theory that stomata maximize CO_2 assimilation per molecule of water vapor lost via transpiration (Medlyn et al., 2011; Bonan et al., 2014; Franks et al., 2017; Miner et al., 2017; Franks et al., 2018). Medlyn et al. (2011) reconciled the

15 empirical widely utilized Ball-Berry model with a theoretical framework optimizing ribulose 1,5 bisphosphate (RuBP) regeneration-limited photosynthesis. However, such methods of water use efficiency optimization do not account for stomatal closure as a result of soil moisture stress. Bonan et al. (2014) further developed a model considering water use efficiency optimization and water transport between the soil, plant, and atmosphere. Although this model provides a physiological and mechanistic basis for stomatal behaviour, it is heavily parameterized, relying on inputs of plant and soil parameters that could

20 be expected to vary significantly across ecosystem types. For this reason, we view these methods as aspirational for incorporation into atmospheric global CTMs. We find the relative simplicity of the Emberson approach more useful for the purpose and scope of parameters for large scale atmospheric models.

5.2 Implications for modelling ozone

NO_x, as well as O_3, deposition budgets are frequently calculated through inferential methods whereby the deposition

25 velocity is constrained with ambient observations (Holland et al., 2005; Geddes and Murphy, 2014). These inferential models are often complicated by the fast reaction of the NO_2-NO-O_3 triad, making it difficult to separate chemical and physical processes. Further, these inferential models for determining dry deposition constrained with observations of chemical concentrations and eddy covariance measurements of fluxes are difficult to interpret because of similar chemical and turbulent timescales (Min et al., 2014; Geddes and Murphy, 2014). Emission of NO from soils, rapid chemical conversion to NO_2, and

30 subsequent in-air reactions of NO_x must be evaluated accurately in in order to correctly infer NO_x and O_3 atmosphere-biosphere exchange from observations. Our multilayer canopy model applies a simple method of representing these processes and evaluating the separate effects of chemistry and dry deposition on the NO_x budget in forests.

Since the foliar deposition of NO_2 reduces the NO_x lifetime and NO_x that is transported out of the canopy, it will also reduce the amount of ozone that is produced both within and above the canopy. Ozone production efficiency (OPE) in the canopy is calculated using Eq.24–26:

$$L(\text{NO}_x) = L_{NO_x \rightarrow Dep} + L_{NO_x \rightarrow RONO_2} + L_{NO_x \rightarrow HNO_3}, \tag{24}$$

$$P(\text{O}_3) = k_{HO_2+NO}[\text{HO}_2][\text{NO}] + k_{CH_3O_2+NO}[\text{CH}_3\text{O}_2][\text{NO}] + (1-\alpha)k_{RO_2+NO}[\text{RO}_2][\text{NO}], \tag{25}$$

$$\text{OPE} = \frac{P(\text{O}_3)}{L(\text{NO}_x)}, \tag{26}$$

where $P(\text{O}_3)$ is the ozone production rate and $L(\text{NO}_x)$ is the NO_x loss rate. The effect of stomatal conductance to NO_2 on OPE is shown in Figure 6c. An increase in g_{max} from 0 to 0.3 cm s^{-1} results in a decrease in OPE for the planetary boundary layer from 24.0 to 20.7 (~14%), and a decrease to 17.0 (~30%) if g_{max} is 1.4 cm s^{-1}. This is similar to OPE calculations that have been reported for forests and environments with NO_x mixing ratios less than 1 ppb and heavily influenced by BVOC emissions (Marion et al., 2001;Browne and Cohen, 2012;Ninneman et al., 2017).

NO_x deposition and the in-canopy chemistry of NO_2-NO-O_3 also impacts O_3 production and removal. O_3 deposition is frequently inferred from measurements of O_3 concentrations or eddy-covariance measurements (Wesely and Hicks, 2000; Kavassalis and Murphy, 2017). However, because NO_2 has a direct impact on ozone production, deposition of NO_2 can affect inferences of O_3 deposition from observations. The 14% reduction of OPE and more than a 20% reduction in daytime NO_x resulting from an increase in g_{max} from 0 to 0.3 cm s^{-1} can cause a parallel decrease in O_3 concentrations and fluxes independent from O_3 chemical loss or deposition. Thus, deposition of NO_2 must be taken into account when evaluating O_3 deposition losses from observed canopy fluxes.

5.3 Implications for near-urban forests

The analysis above suggests that the relative importance of chemical sinks and deposition will vary with NO_x concentration. To evaluate the relative importance of NO_2 foliar deposition and chemistry as a function of NO_x mixing ratio, a simplified 1-box model was also constructed with a simplified reaction scheme (Table S3), VOC reactivity of 8 s^{-1}, α of 0.075, and a HO_x ($HO_x \equiv OH + HO_2$) production rate (P_{HO_x}) of 2×10^6 molecules cm^{-3}s^{-1}. RO_2, OH, and HO_2 were solved for steady-state concentrations and NO_x loss pathways were calculated via Eq. 27–30.

$$D_{NO_x} = LAI \cdot V_d \cdot \frac{h_{can}}{h_{PBL}}[NO_2] \tag{27}$$

where h_{can} is the canopy height (15m), h_{PBL} is the planetary boundary layer height (1000 m), and LAI is 0.8 m^2/m^2.

$$P_{HNO_3} = k_{OH+NO_2}[OH][NO_2] \tag{28}$$

$$P_{ANs} = \alpha k_{RO_2+NO}[RO_2]fNO \tag{29}$$

where

$$fNO = \frac{k_{RO_2+NO}[NO]}{k_{RO_2+NO}[NO] + k_{RO_2+HO_2}[HO_2] + k_{RO_2+RO_2}[RO_2]} \tag{30}$$

The results from this simplified box model are shown in Figure 9 and agree well with our 1D multi-box model near 10 ppb NO_x (Fig S7). With deposition set to zero, nitric acid formation becomes a more significant sink of NO_x than alkyl nitrate formation at around 1 ppb, and nitric acid formation accounts for greater than 70% of the total loss at 100 ppb. With a deposition pathway included, deposition acts as the dominant NO_x sink above 30 ppb and at 10 ppb deposition and AN formation are each 20% of the NO_x sink. Deposition is approximately 10% of the sink over a wide range of concentrations. Forests in close proximity to urban centers (Fig S9) may result in a substantial local decrease in NO_x (Fig S8, Fig 10). Although the influence of urban or near-urban trees on NO_x concentrations would be heavily dependent on meteorological factors (i.e. wind speed and direction), proximity to emission sources, and LAI, it may have some importance on a local or neighborhood scale. This effect may be relevant for understanding and predicting the effects of NO_x reduction policies within and near cities. It may also be useful in considering as a direct nitrogen input to the biosphere, not mediated by soil processes.

6 Conclusions

We have constructed a 1D multi-box model with representations of chemistry and vertical transport to evaluate the impact of leaf-level processes on canopy-scale concentrations, lifetimes, and canopy fluxes of NO_x. Our model is able to closely replicate canopy fluxes and above-canopy NO_x daytime mixing ratios during two field campaigns taking place in a Sierra Nevada pine forest (BEARPEX-2009) and a northern Michigan mixed hardwood forest (UMBS-2012). We conclude that the widely used canopy reduction factor approach to describing soil NO_x removal from the atmosphere within plant canopies is consistent with a process-based model that utilizes stomatal uptake and we recommend that the CRF parameter be replaces with stomatal models for NO_x uptake.

We demonstrate with our 1D multi-box model that NO_2 deposition provides a mechanistic explanation behind canopy reduction factors (CRFs) that are widely used in CTMs. We predict a maximum of ~60% reduction in the fraction of soil-emitted NO_x ventilated through the canopy when stomatal conductances are greater than 0.075 cm s^{-1}, consistent with the range of global CRFs used in current CTMs (Jacob and Wofsy, 1990;Yienger and Levy, 1995). Our model also predicts that changes in g_{max} have a greater overall impact on canopy NO_x fluxes at larger leaf resistances to uptake (slower foliar uptake). In the range for g_{max} of ~0–0.5 cm s^{-1}, errors or variability in stomatal conductance can have a large impact on the predicted canopy concentrations and fluxes of NO_x, which would in turn have large impact on concentrations and fluxes of O_3. This range of deposition velocities describes the range of uptake rates measured for many tree species and forest ecosystems (Hanson and Lindberg, 1991; Rondon and Granat, 1994; Hereid and Monson, 2001; Teklemariam and Sparks, 2006; Pape et al., 2008; Chaparro-Suarez et al., 2011; Delaria et al., 2018. Model calculations also predict a similar trend on the lifetimes of NO_x, with a maximum reduction in the NO_x lifetime by ~4 hrs (>40%) compared with no deposition.

The large effect that small changes in stomatal conductance can have on NO_x lifetimes, concentrations, budget, and O_3 production makes it very important to accurately parameterize in atmospheric models. Most global scale chemistry transport models parameterize stomatal conductance using the resistance in-series approach similar to that developed by Wesely (1989)

(Jacob and Wofsy, 1990; Wang and Leuning, 1998; Ganzeveld et al., 2002; Verbeke et al., 2015. These do no account for the effects of VPD, SWP, CO_2 mixing ratio, or other factors known to influence stomatal conductance (Hardacre et al., 2015). We show that incorporating vapor pressure deficit and soil water potential—using the parameterization of Emberson et al. (2000)—has a substantial impact on predicted NO_2 deposition, with the percent of soil NO_x removed within the canopy increasing from 18% to 30% in wet (low VPD and high SWP) conditions compared to dry conditions in the location of BEARPEX-2009. Under the Wesely model, where stomatal conductance is parameterized only with temperature and solar radiation, the predicted deposition velocity would be nearly identical between wet and dry days and between the spring and fall in semi-arid regions (e.g. much of the western United States. The dominant effect of stomatal opening on NO_2 deposition causes an important time of day and seasonal behaviour that should be extensively explored.

Acknowledgements. We wish to gratefully acknowledge financial support from the National Science Foundation (NSF, AGS-1352972). This study was supported by NOAA Climate Program Office's Atmospheric Chemistry, Carbon Cycle, and Climate program NA18OAR4310117. Additional support was provided by an NSF Graduate Research Fellowship to Erin R. Delaria. We would also like to give a special thanks to Jennifer G. Murphy, University of Toronto and Jeffrey Geddes, Boston University for providing data from the UMBS field site; and J. Geddes for constructive comments that improved the manuscript.

References

Altimir, N., Tuovinen, J.-P., Vesala, T., Kulmala, M., Hari, P.: Measurements of ozone removal by Scots pine shoots: calibration of a stomatal uptake model including the non-stomatal component, Atmospheric Environment, 38(15), 2387–2398, https://doi.org/10.1016/j.atmosenv.2003.09.077, 2004.

5   Ammann, M., Ballmoos, P.V., Stalder, M., Suter, M., Brunold, C.: Uptake and assimilation of atmospheric NO2 — N by spruce needles (Picea abies): A field study. Water, Air, and Soil Pollution, 85(3), 1497–1502, https://doi.org/10.1007/BF00477193, 1995.

Anderegg, W. R., Wolf, A., Arango-Velez, A., Choat, B., Chmura, D. J., Jansen, S., Kolb, T., Li, S., Meinzer, F., Pita, P., Resco de Dios, V., Sperry, J. S., Wolfe, B. T., and Pacala, S.: Plant water potential improves prediction of empirical stomatal
10   models, PLoS ONE, 12, e0185 481f, https://doi.org/10.1371/journal.pone.0185481, 2017.

Baldocchi, D. D., Hicks, B. B., and Camara, P.: A Canopy Stomatal-Resistance Model for Gaseous Deposition to Vegetated Surfaces, Atmos. Environ., 21, 91–101, https://doi.org/10.1016/0004-6981(87)90274-5, 1987.

Beedlow, P.A., Lee, E.H., Tingey, D.T., Waschmann, R.S., Burdick, C.A.:The importance of seasonal temperature and moisture patterns on growth of Douglas-fir in western Oregon, USA, Agr Forest Meteorol, 169, 174-185,
15   https://doi.org/10.1016/j.agrformet.2012.10.010, 2013.

Bonan, G. B., Williams, M., Fisher, R. A., and Oleson, K. W.: Modelling stomatal conductance in the earth system: linking leaf water-use efficiency and water transport along the soil–plant–atmosphere continuum, Geosci. Model Dev., 7, 2193-2222, https://doi.org/10.5194/gmd-7-2193-2014, 2014.

Breuninger, C., Meixner, F. X., and Kesselmeier, J.: Field investigations of nitrogen dioxide (NO2) exchange between plants
20   and the atmosphere, Atmos. Chem. Phys., 13, 773-790, https://doi.org/10.5194/acp-13-773-2013, 2013.

Browne, E. C. and Cohen, R. C.: Effects of biogenic nitrate chemistry on the NOx lifetime in remote continental regions, Atmos. Chem. Phys., 12, 11917-11932, https://doi.org/10.5194/acp-12-11917-2012, 2012.

Büker, P., Emberson, L.D., Ashmore, M.R., Cambridge, H.M., Jacobs, C.M.J., Massman, W.J., Muller, J., Nikolov, N., Novak, K., Oksanen, E., Schaub, M., and de la Torre, D.Comparison of different stomatal conductance algorithms for ozone flux
25   modelling, Environmental Pollution, 146(3), 726–735, https://doi.org/10.1016/j.envpol.2006.04.007, 2007.

Büker, P., Morrissey, T., Briolat, A., Falk, R., Simpson, D., Tuovinen, J.-P., Alonso, R., Barth, S., Baumgarten, M., Grulke, N., Karlsson, P. E., King, J., Lagergren, F., Matyssek, R., Nunn, A., Ogaya, R., Peñuelas, J., Rhea, L., Schaub, M., Uddling, J., Werner, W., and Emberson, L. D.: DO3SE modelling of soil moisture to determine ozone flux to forest trees, Atmos. Chem. Phys., 12, 5537-5562, https://doi.org/10.5194/acp-12-5537-2012, 2012.

30   Burkholder, J.B., Sander, S.P., Abbatt, J., Barker, J.R., Huie, R.E., Kolb, C. E., Kurylo, M. J., Orkin, V. L., Wilmouth, D. M. andWine P. H.:Chemical Kinetics and Photochemical Data for Use in Atmospheric Studies, Evaluation No. 18, JPL Publication 15-10, Jet Propulsion Laboratory, Pasadena, http://jpldataeval.jpl.nasa.gov, 2015.

Chaparro-Suarez, I. G., Meixner, F. X., and Kesselmeier, J.: Nitrogen dioxide (NO2) uptake by vegetation controlled by atmospheric concentrations and plant stomatal aperture, Atmos. Environ., 45, 5742–5750,
35   https://doi.org/10.1016/j.atmosenv.2011.07.021, 2011.

Chaves, M.M.: How Plants Cope with Water Stress in the Field? Photosynthesis and Growth, Annals of Botany, 89(7), 907–916, https://doi.org/10.1093/aob/mcf105, 2002.

Crutzen, P.J.: The Role of NO and NO2 in the Chemistry of the Troposphere and Stratosphere. Annual Review of Earth and Planetary Sciences, 7(1), 443–472, https://doi.org/10.1146/annurev.ea.07.050179.002303,1979.

5   Delaria, E. R., Vieira, M., Cremieux, J., and Cohen, R. C.: Measurements of NO and NO2 exchange between the atmosphere and Quercus agrifolia, Atmos. Chem. Phys., 18, 14161-14173, https://doi.org/10.5194/acp-18-14161-2018, 2018.

Emberson, L., Ashmore, M., Cambridge, H., Simpson D., Tuovinen, J.-P.: Modelling stomatal ozone flux across Europe, Environmental Pollution, 109(3), 403–413, https://doi.org/10.1016/S0269-7491(00)00043-9, 2000.

Emberson, L.D.: Defining and mapping relative potential sensitivity of European vegetation to ozone. Ph.D. Thesis, Imperial
10 College, University of London, UK, 1997.

Fares S., Matteucci G., Mugnozza G.S., Morani A., Calfapietra C., Salvatori E., Fursao, L., Manes, F., and Loreto F.: Testing of models of stomatal ozone fluxes with field measurements in a mixed Mediterranean forest. Atmospheric Environment, 67, 242–251, https://doi.org/10.1016/j.atmosenv.2012.11.007, 2013.

Fenn M.E., et al. (1998) Nitrogen Excess in North American Ecosystems: Predisposing Factors, Ecosystem Responses, and
15 Management Strategies. Ecological Applications 8(3):706.

Franks, P.J., Berry, J.A., Lombardozzi, D.L., Bonan, G.B.: Stomatal Function across Temporal and Spatial Scales: Deep-Time Trends, Land-Atmosphere Coupling and Global Models, Plant Physiology, 174, 583-602, https://doi.org/10.1104/pp.17.00287, 2017

Franks, P.J., Bonan, G.B., Berry, J.A., et al.: Comparing optimal and empirical stomatal conductance models for application
20 in Earth system models. Glob Change Biol., 24: 5708– 5723. https://doi.org/10.1111/gcb.14445, 2018.

Galloway, J. N., Dentener, F. J., Capone, D. G., Boyer, E. W., Howarth, R. W., Seitzinger, S. P., Asner, G.P., Cleveland, C.C., Green, P.A., Holland, E.A., Karl, D.M., Michaels, A.F., Porter, J.H., Townsend, A.R., Vörösmarty, C. J.: Nitrogen cycles: Past, present, and future. Biogeochemistry, 70(2), 153-226, https://doi.org/10.1007/s10533-004-0370-0, 2004.

Ganzeveld, L. N., Lelieveld, J., Dentener, F. J., Krol, M. C., and Roelofs, G. J.: Atmosphere-biosphere trace gas exchanges
25 simulated with a single-column model, J. Geophys. Res.-Atmos., 107, 4297, https://doi.org/10.1029/2001jd000684, 2002.

Gao W, Wesely ML, Doskey PV (1993) Numerical modelling of the turbulent diffusion and chemistry of NOx, O3, isoprene, and other reactive trace gases in and above a forest canopy. Journal of Geophysical Research: Atmospheres 98(D10):18339–18353.

Geddes, J. A. and Murphy, J. G.: Observations of reactive nitrogen oxide fluxes by eddy covariance above two midlatitude
30 North American mixed hardwood forests, Atmos. Chem. Phys., 14, 2939-2957, https://doi.org/10.5194/acp-14-2939-2014, 2014.

Guenther, A., Hewitt, C. N., Erickson, D., Fall, R., Geron, C., Graedel, T., Harley, P., Klinger, L., Lerdau, M. T., McKay, W.A., Pierce, T., Scholes, B., Steinbrecher, R., Tallamraju, R., Taylor, J., and Zimmerman, P.: A global model of natural volatile organic compound emissions, J. Geophys. Res., 100, 8873–8892, https://doi.org/10.1029/94JD02950, 1995.

Gunderson, C. A., Sholtis, J. D., Wullschleger, S. D., Tissue, D. T., Hanson, P. J. and Norby, R. J.: Environmental and stomatal control of photosynthetic enhancement in the canopy of a sweetgum (Liquidambar styraciflua L.) plantation during 3 years of CO2 enrichment, Plant, Cell & Environment, 25, 379-393, https://doi.org/10.1046/j.0016-8025.2001.00816.x, 2002.

Hanson, P. J. and Lindberg, S. E.: Dry Deposition of Reactive Nitrogen-Compounds – a Review of Leaf, Canopy and Non-Foliar Measurements, Atmos. Environ. A-Gen., 25, 1615–1634, https://doi.org/10.1016/0960-1686(91)90020-8, 1991.

Hardacre, C., Wild, O., and Emberson, L.: An evaluation of ozone dry deposition in global scale chemistry climate models, Atmos. Chem. Phys., 15, 6419-6436, https://doi.org/10.5194/acp-15-6419-2015, 2015.

Hereid, D. P. and Monson, R. K.: Nitrogen oxide fluxes between corn (Zea mays L.) leaves and the atmosphere, Atmos. Environ., 35, 975–983, https://doi.org/10.1016/S1352-2310(00)00342-3, 2001.

Holland, E.A., Braswell, B.H., Lamarque, J.-F., Townsend, A., Sulzman, J., Müller, J.-F., Dentener, F., Brasseur, G., Levy, H.II, Penner, J.E., and Roelofs, G.-J.: Variations in the predicted spatial distribution of atmospheric nitrogen deposition and their impact on carbon uptake by terrestrial ecosystems. Journal of Geophysical Research: Atmospheres 102(D13):15849–15866, https://doi.org/10.1029/96JD03164, 1997.

Holland, E.A., Braswell, B.H., Sulzman, J., Lamarque, F.: Nitrogen deposition onto the United States and western Europe: Synthesis of observations and models, Ecol Appl, 15, 38-57, https://doi.org/10.1890/03-5162, 2005.

Hubbard, R.M., Ryan, M.G., Stiller, V., and Sperry, J.S.: Stomatal conductance and photosynthesis vary linearly with plant hydraulic conductance in ponderosa pine, Plant, Cell & Environment, 24, 113-121, https://doi.org/10.1046/j.1365-3040.2001.00660.x, 2001.

Ishikawa, C.M. and Bledsoe, C.: Seasonal and diurnal patterns of soil water potential in the rhizosphere of blue oaks: evidence for hydraulic lift, Oecologia, 125(4), 459–465, https://doi.org/10.1007/s004420000470, 2000.

Jacob D.J. and Wofsy S.C.: Budgets of reactive nitrogen, hydrocarbons, and ozone over the Amazon forest during the wet season. Journal of Geophysical Research, 95(D10),16737, https://doi.org/10.1029/JD095iD10p16737,1990.

Johansson, C.: Pine forest: a negligible sink for atmospheric NOx in rural Sweden, Tellus B, 39B, 426–438, 1987.

Johnson, D., Woodruff, D., Mcculloh, K., Meinzer, F.: Leaf hydraulic conductance, measured in situ, declines and recovers daily: leaf hydraulics, water potential and stomatal conductance in four temperate and three tropical tree species, Tree Physiology, 29(7), 879–887, https://doi.org/10.1093/treephys/tpp031, 2009.

Kavassalis, S.C. and Murphy, J.G.:Understanding ozone-meteorology correlations: A role for dry deposition, Geophysical Research Letters, 44(6), 2922–2931, https://doi.org/10.1002/2016GL071791, 2017.

Keilliher, F. F., Leuning, R., Raupach, M.R., and Schulze, E.-D.: Maximum conductances for evaporation from global vegetation types: Agric. For. Meteorol., 73, 1-16, https://doi.org/10.1016/0168-1923(94)02178-M, 1995.

Madronich S, Flocke S.: The Role of Solar Radiation in Atmospheric Chemistry. The Handbook of Environmental Chemistry Environmental Photochemistry:1–26, 1999.

Mallick, K., Jarvis, A., Fisher, J.B., Tu, K.P., Boegh, E., and Niyogi, D.: Latent Heat Flux and Canopy Conductance Based on Penman–Monteith, Priestley–Taylor Equation, and Bouchet's Complementary Hypothesis, J. Hydrometeor., 14, 419–442, https://doi.org/10.1175/JHM-D-12-0117.1, 2013.

Medlyn, B. E., Duursma, R. A., Eamus, D., Ellsworth, D. S., Prentice, I. C., Barton, C. V., Crous, K. Y., De Angelis, P., Freeman, M. And Wingate, L.: Reconciling the optimal and empirical approaches to modelling stomatal conductance. Global Change Biology, 17, 2134-2144, https://doi.org/10.1111/j.1365-2486.2010.02375.x, 2011.

Min, K.-E., Pusede, S. E., Browne, E. C., LaFranchi, B. W., and Cohen, R. C.: Eddy covariance fluxes and vertical concentration gradient measurements of NO and NO2 over a ponderosa pine ecosystem: observational evidence for within-canopy chemical removal of NOx, Atmos. Chem. Phys., 14, 5495-5512, https://doi.org/10.5194/acp-14-5495-2014, 2014.

Miner, G. L., Bauerle, W. L., and Baldocchi, D. D.: Estimating the sensitivity of stomatal conductance to photosynthesis: a review. Plant, Cell & Environment, 40, 1214– 1238. doi: 10.1111/pce.12871, 2017.

Nguyen, T.B., Crounse, J.D., Teng, A.P., St. Clair, J.M., Paulot, F., Wolfe, G.M., Wennberg, P.O.: Rapid deposition of oxidized biogenic compounds to a temperate forest, Proceedings of the National Academy of Sciences, 112 (5), E392-E401, https://doi.org/10.1073/pnas.1418702112, 2015.

Oren, R., Ellsworth, D.S., Johnsen, K.H., Phillips, N., Ewers, B.E., Maier, C., Schafer, K.V.R., McCarthy, H. Hendrey, G. McNulty, S.G., Katul, G.G.: Soil fertility limits carbon sequestration by forest ecosystems in a CO2-enriched atmosphere, Nature, 411(6836), 469–472, https://doi.org/10.1038/35078064, 2001.

Panek, J.A., Goldstein, A.H.: Response of stomatal conductance to drought in ponderosa pine: implications for carbon and ozone uptake, Tree Physiology, 21(5), 337–344, https://doi.org/10.1093/treephys/21.5.337, 2001.

Pape, L., Ammann, C., Nyfeler-Brunner, A., Spirig, C., Hens, K., and Meixner, F. X.: An automated dynamic chamber system for surface exchange measurement of non-reactive and reactive trace gases of grassland ecosystems, Biogeosciences, 6, 405-429, https://doi.org/10.5194/bg-6-405-2009, 2009.

Prior, L.D, Eamus, D., Duff, G.A.: Seasonal and Diurnal Patterns of Carbon Assimilation, Stomatal Conductance and Leaf Water Potential in Eucalyptus tetrodonta Saplings in a Wet - Dry Savanna in Northern Australia, Australian Journal of Botany, 45(2), 241, https://doi.org/10.1071/BT96017, 1997.

Romer, P. S., Duffey, K. C., Wooldridge, P. J., Allen, H. M., Ayres, B. R., Brown, S. S., Brune, W. H., Crounse, J. D., de Gouw, J., Draper, D. C., Feiner, P. A., Fry, J. L., Goldstein, A. H., Koss, A., Misztal, P. K., Nguyen, T. B., Olson, K., Teng, A. P., Wennberg, P. O., Wild, R. J., Zhang, L., and Cohen, R. C.: The lifetime of nitrogen oxides in an isoprene-dominated forest, Atmos. Chem. Phys., 16, 7623-7637, https://doi.org/10.5194/acp-16-7623-2016, 2016.

Rondon, A. and Granat, L.: Studies on the Dry Deposition of NO2 to Coniferous Species at Low NO2 Concentrations, Tellus B, 46, 339–352, https://doi.org/10.1034/j.1600-0889.1994.t01-4-00001.x, 1994.

Ryan, M., Bond, B., Law, B. et al.: Transpiration and whole-tree conductance in ponderosa pine trees of different heights, Oecologia 124, 553-560, https://doi.org/10.1007/s004420000403, 2000.

Rydsaa, J., Stordal, F., Gerosa, G., Finco, A., Hodnebrog Ø.: Evaluating stomatal ozone fluxes in WRF-Chem: Comparing ozone uptake in Mediterranean ecosystems, Atmospheric Environment, 143, 237–248, https://doi.org/10.1016/j.atmosenv.2016.08.057, 2016.

Seok, B., Helmig, D., Ganzeveld, L., Williams, M. W., and Vogel, C. S.: Dynamics of nitrogen oxides and ozone above and within a mixed hardwood forest in northern Michigan, Atmos. Chem. Phys., 13, 7301-7320, https://doi.org/10.5194/acp-13-7301-2013, 2013.

Simpson, D., Benedictow, A., Berge, H., Bergström, R., Emberson, L. D., Fagerli, H., Flechard, C. R., Hayman, G. D., Gauss, M., Jonson, J. E., Jenkin, M. E., Nyíri, A., Richter, C., Semeena, V. S., Tsyro, S., Tuovinen, J.-P., Valdebenito, Á., and Wind, P.: The EMEP MSC-W chemical transport model – technical description, Atmos. Chem. Phys., 12, 7825-7865, https://doi.org/10.5194/acp-12-7825-2012, 2012.

5   Stern, M.A., Anderson, F.A., Flint, L.E., Flint, A.L.: Soil moisture datasets at five sites in the central Sierra Nevada and northern Coast Ranges, California. Data Series, https://doi.org/10.3133/ds1083, 2018.

Teklemariam, T. A. and Sparks, J. P.: Leaf fluxes of NO and NO2 in four herbaceous plant species: The role of ascorbic acid, Atmos. Environ., 40, 2235–2244, https://doi.org/10.1016/j.atmosenv.2005.12.010, 2006.

Thoene, B., Schroder, P., Papen, H., Egger, A., and Rennenberg, H.: Absorption of Atmospheric No2 by Spruce (Picea-Abies
10   L Karst) Trees 1, NO2 Influx and Its Correlation with Nitrate Reduction, New Phytol., 117, 575–585, https://doi.org/10.1111/j.1469-8137.1991.tb00962.x, 1991.

Townsend A.R., Braswell B.H., Holland E.A., and Penner J.E.: Spatial and Temporal Patterns in Terrestrial Carbon Storage Due to Deposition of Fossil Fuel Nitrogen. Ecological Applications, 6(3), 806–814, https://doi.org/10.2307/2269486, 1996.

Verbeke, T., Lathière, J., Szopa, S., and de Noblet-Ducoudré, N.: Impact of future land-cover changes on HNO3 and O3
15   surface dry deposition, Atmos. Chem. Phys., 15, 13555-13568, https://doi.org/10.5194/acp-15-13555-2015, 2015.

Vinken, G. C. M., Boersma, K. F., Maasakkers, J. D., Adon, M., and Martin, R. V.: Worldwide biogenic soil NOx emissions inferred from OMI NO2 observations, Atmos. Chem. Phys., 14, 10363-10381, https://doi.org/10.5194/acp-14-10363-2014, 2014.

Vitousek, P. M., Aber, J. D., Howarth, R. W., Likens, G. E., Matson, P. A., Schindler, D. W., Schlesinger, W. H. and Tilman,
20   D. G.: Human Alteration of the Global Nitrogen Cycle: Sources and Consequences, Ecological Applications, 7(3), 737-750, https://doi.org/10.1890/1051-0761(1997)007[0737:HAOTGN]2.0.CO;2, 1997.

Wang, Y., Jacob D.J., and Logan, J.A.: Global simulation of tropospheric O3-NOx-hydrocarbon chemistry: 1. Model formulation, Journal of Geophysical Research: Atmospheres,103(D9),10713–10725, https://doi.org/10.1029/98JD00158, 1998a.

25   Wang, Y., Logan, J.A., Jacob D.J.: Global simulation of tropospheric O3-NOx-hydrocarbon chemistry: 2. Model evaluation and global ozone budget,Journal of Geophysical Research: Atmospheres,103(D9),10727–10755, https://doi.org/10.1029/98JD00157, 1998b.

Wang, Y.-P. and Leuning, R.: A two-leaf model for canopy conductance, photosynthesis and partitioning of available energy I, Agricultural and Forest Meteorology, 91(1-2), 89–111, https://doi.org/10.1016/S0168-1923(98)00061-6, 1998.

30   Wesely, M. L. and Hicks, B. B.: A review of the current status of knowledge on dry deposition, Atmos. Environ., 34, 2261–2282, 2000.

Wesely, M.: Parameterization of surface resistances to gaseous dry deposition in regional-scale numerical models, Atmospheric Environment, 23(6),1293–1304, https://doi.org/10.1016/0004-6981(89)90153-4, 1989.

Wild, O.: Modelling the global tropospheric ozone budget: exploring the variability in current models, Atmos. Chem. Phys.,
35   7, 2643-2660, https://doi.org/10.5194/acp-7-2643-2007, 2007.

Williams, M. , Rastetter, E. B., Fernandes, D. N., Goulden, M. L., Wofsy, S. C., Shaver, G. R., Melillo, J. M., Munger, J. W., Fan, S. And Nadelhoffer, K. J.: Modelling the soil-plant-atmosphere continuum in a Quercus-Acer stand at Harvard Forest: the regulation of stomatal conductance by light, nitrogen and soil/plant hydraulic properties. Plant, Cell and Environment 19(8):911–927, https://doi.org/10.1111/j.1365-3040.1996.tb00456.x, 1996.

5   Wolfe, G. M. and Thornton, J. A.: The Chemistry of Atmosphere-Forest Exchange (CAFE) Model – Part 1: Model description and characterization, Atmos. Chem. Phys., 11, 77-101, https://doi.org/10.5194/acp-11-77-2011, 2011.

Wolfe, G. M., Thornton, J. A., Bouvier-Brown, N. C., Goldstein, A. H., Park, J.-H., McKay, M., Matross, D. M., Mao, J., Brune, W. H., LaFranchi, B. W., Browne, E. C., Min, K.-E., Wooldridge, P. J., Cohen, R. C., Crounse, J. D., Faloona, I. C., Gilman, J. B., Kuster, W. C., de Gouw, J. A., Huisman, A., and Keutsch, F. N.: The Chemistry of Atmosphere-Forest Exchange
10 (CAFE) Model – Part 2: Application to BEARPEX-2007 observations, Atmos. Chem. Phys., 11, 1269-1294, https://doi.org/10.5194/acp-11-1269-2011, 2011.

Yienger, J.J. and Levy, H.: Empirical model of global soil-biogenic NOx emissions, Journal of Geophysical Research, 100(D6), 11447-11464, https://doi.org/10.1029/95JD00370, 1995.

Zhang, L., Padro, J., Walmsley, J.: A multi-layer model vs single-layer models and observed O3 dry deposition
15 velocities, Atmospheric Environment, 30(2), 339–345, https://doi.org/10.1016/1352-2310(95)00286-8,1996.

Tables

Table 1: Parameters used in the model for comparison to observations from UMBS and BEARPEX-2009

Parameter	Symbol	UMBS	BEARPEX
Canopy height	h_{can}	20 m	10 m
Total leaf area index	LAI	3.5 m^2/m^2	5.1 m^2/m^2
Radiation extinction coefficient	k_{rad}	0.4	0.4
Diffusion timescale ratio	τ/T	2	2
Friction velocity	$u*$	61 cm s^{-1}	61 cm s^{-1}
Maximum NO emission flux	eNO$_{max}$	0.7 ppt ms^{-1}	3 ppt ms^{-1}
Minimum NO emission flux	eNO$_{miin}$	0.3 ppt ms^{-1}	1 ppt ms^{-1}
VOC basal emission flux	E_b	5 ppb m s^{-1}	11 ppb m s^{-1}
Integration interval	Δt	2	2
OH + VOC rate constant (cm^3 molecules^{-1} s^{-1})	kOH	9.8×10^{-11}	8.7×10^{-11}
NO$_3$ + VOC rate constant (cm^3 molecules^{-1} s^{-1})	kNO$_3$	7.0×10^{-13}	1.7×10^{-14}
Minimum daily temperature		15 °C	17 °C
Maximum daily temperature		23 °C	27 °C
Maximum daily relative humidity		85%	65%
Minimum daily relative humidity		65%	30%
Maximum daily soil water potential		-0.05 MPa	-0.8 MPa
Minimum daily soil water potential		-0.25 MPa	-1.0 MPa

Table 2: Parameters used in the Emberson model for stomatal conductance

	UMBS	reference	BEARPEX	reference
g_{max} (cm s^{-1})	0.2	Büker et al. 2012	0.3	Altimir et al. 2003
f_{min}	0.05	Büker et al. 2012	0.03	Büker et al. 2012
$Light\_a$	0.001	Büker et al. 2012	0.001	This study
T_{max} (°C)	33	Büker et al. 2012	35	Altimir et al. 2003
T_{min} (°C)	5	Büker et al. 2012	5	Altimir et al. 2003
T_{opt} (°C)	16	Büker et al. 2012	20	Altimir et al. 2003
VPD_{min} (kPa)	3.1	Büker et al. 2012	4	Ryan et al. 2000, Hubbard et al. 2001, Kolb and Stone 1999
VPD_{max} (kPa)	1.1	Büker et al. 2012	1.5	Ryan et al. 2000, Hubbard et al. 2001, Kolb and Stone 1999
SWP_{max} (MPa)	-1.0	Emberson et al. 2000	-1.0	Anderegg et al. 2017
SWP_{min} (MPa)	-1.9	Emberson et al. 2000	-2.0	Anderegg et al. 2017

Figures
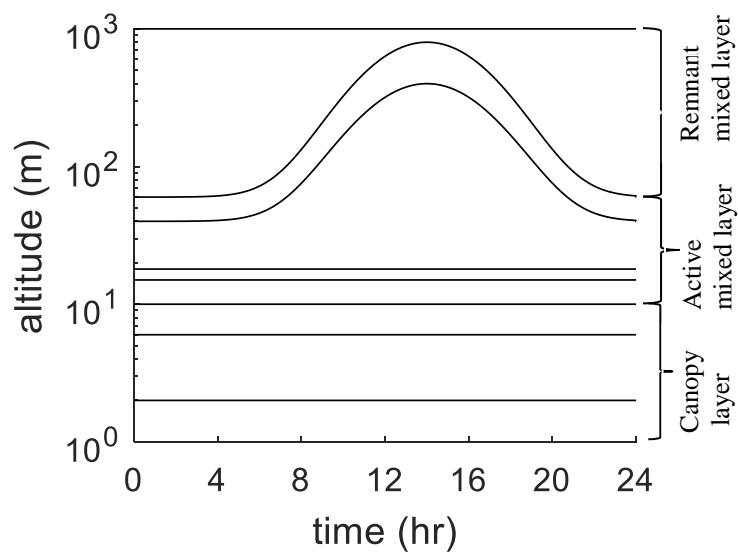
Figure 1: Planetary boundary dynamics in the 1D multibox model. The model domain consists of three boxes in the canopy layer, four in the active mixed layer, and one in the residual mixed layer. The lower five boxes have fixed heights, while the sixth and seventh boxes evolve throughout the day, in the form of a Gaussian function.
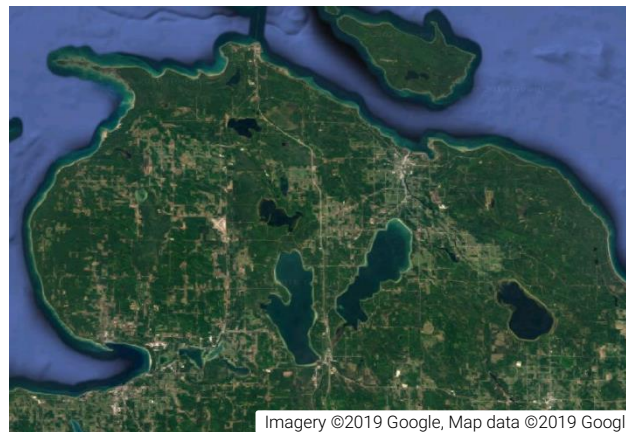
Figure 2: Satellite images showing the locations of (a) the BEARPEX-2009 campaign and (b) the University of Michigan Biological Station (UMBS). Measurements of chemical species and local meteorological variables from the two campaigns were used to validate our 1D canopy multibox model.

a)

b)

c)

d)
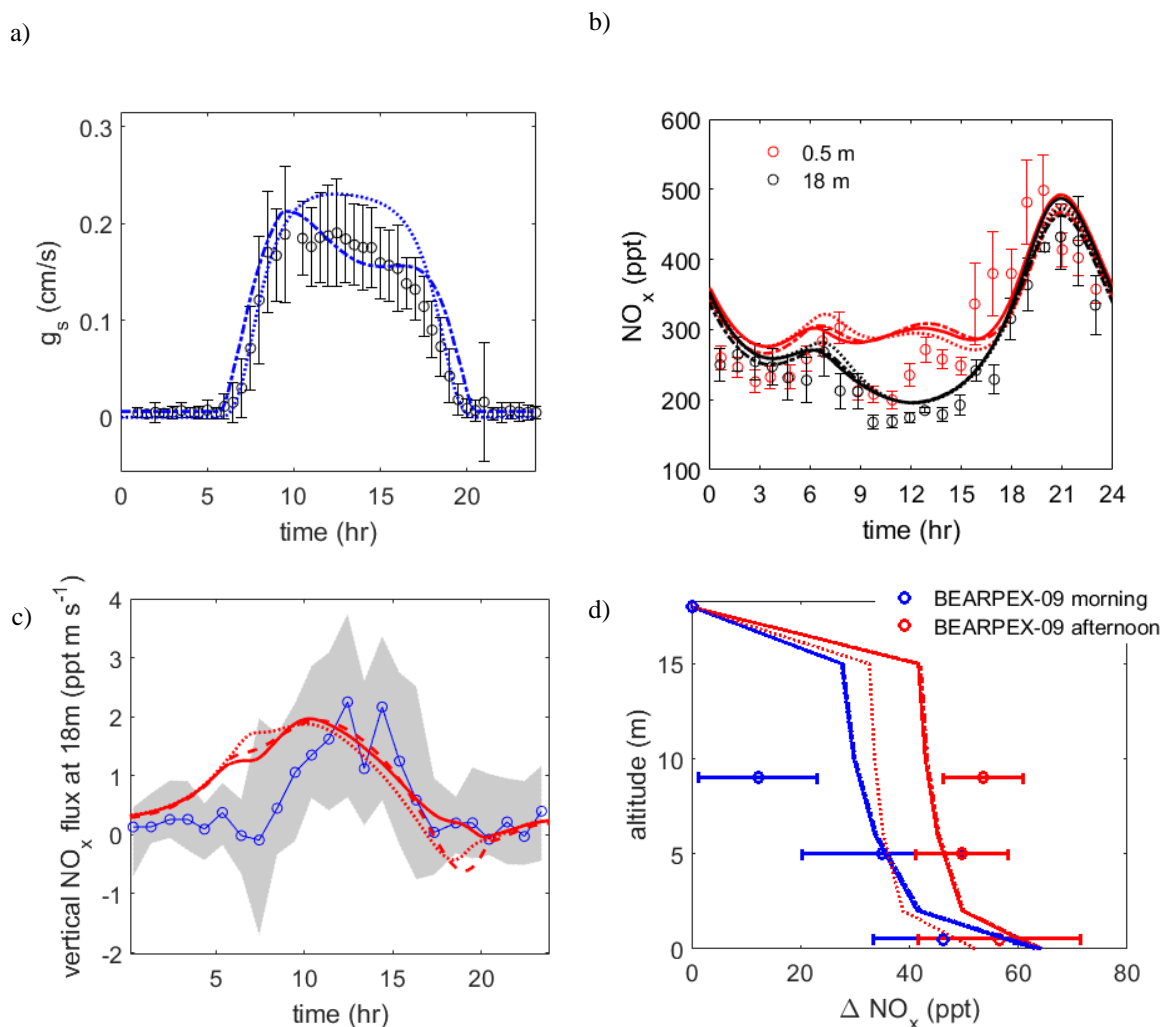
Figure 3: (a) Comparison of 1-hr mean averages of observed stomatal conductances during BEARPEX-2009 (black circles) to stomatal conductances modeled using the Wesely (dotted blue) and Emberson (dashed blue) schemes for June 30, 2009. **(b)** NO_x mixing ratios at 18 m (black) and 0.5 m (red) from observations (circles) and modeled using observed stomatal conductances (solid lines) and the Wesely (dotted lines) and Emberson (dashed lines) parameterizations. **(c)** Observations of vertical fluxes (blue circles) and fluxes modeled using observed stomatal conductances (solid line) or the Wesely (dotted line) and Emberson (dashed line) parameterizations. The grey shaded area gives the interquartile range of the observed flux data for hourly bins. **(d)** Averaged observations of in-canopy NO_x enhancements (circles) in the morning (blue) and afternoon (red) compared with modeled NO_x enhancements using measured canopy conductances (solid lines), and the Wesely (dotted lines) and Emberson (dashed lines) scenarios. Observations from BEARPEX-2009 are from Min et al., (2014). Error bars represent standard errors of the mean.
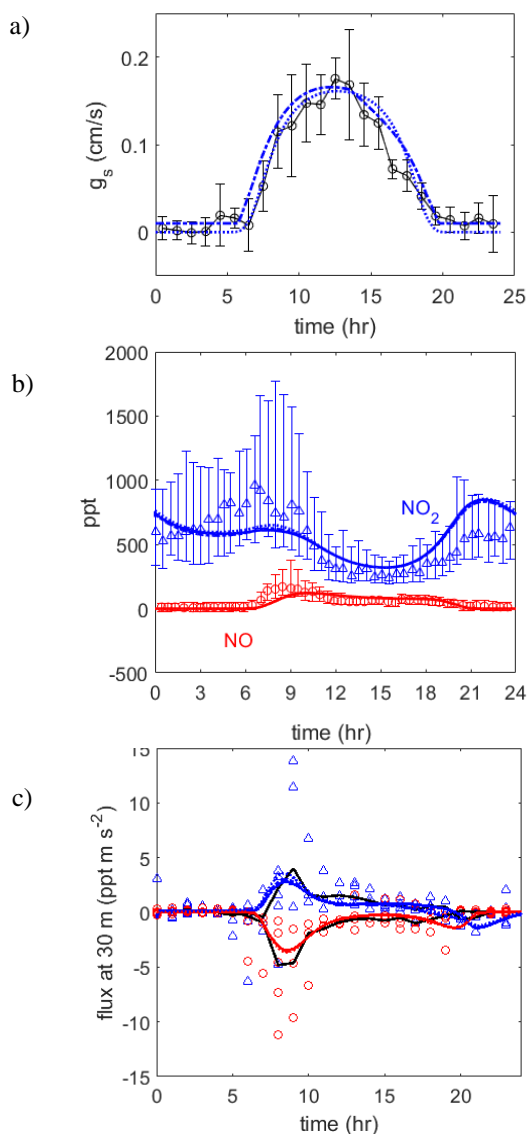
Figure 4: (a) Comparison of averaged observed stomatal conductances at UMBS-2012 (black circles) and modeled stomatal conductances using the Wesely (dotted line) and Emberson (dashed line) scenarios for August 8, 2012. Error bars represent standard deviations of 1-hr averaged values. (b) Observations of NO (red circles) and NO₂ (blue triangles) mixing ratios at 30 m during UMBS-2012 and modeled NO (red) and NO₂ (blue) mixing ratios using measured stomatal conductances (solid lines) and the Wesely (dotted lines) and Emberson (dashed lines) parameterizations. Error bars give the interquartile range of flux data. (c) Median (black lines) and hourly-averaged NO (red circles) and NO2 (blue triangles) observed vertical fluxes at 30 m compared to modeled NO (red) and NO2 (blue) fluxes using measured stomatal conductances (solid lines) and the Wesely (dotted lines) and Emberson (dashed lines) parameterizations.
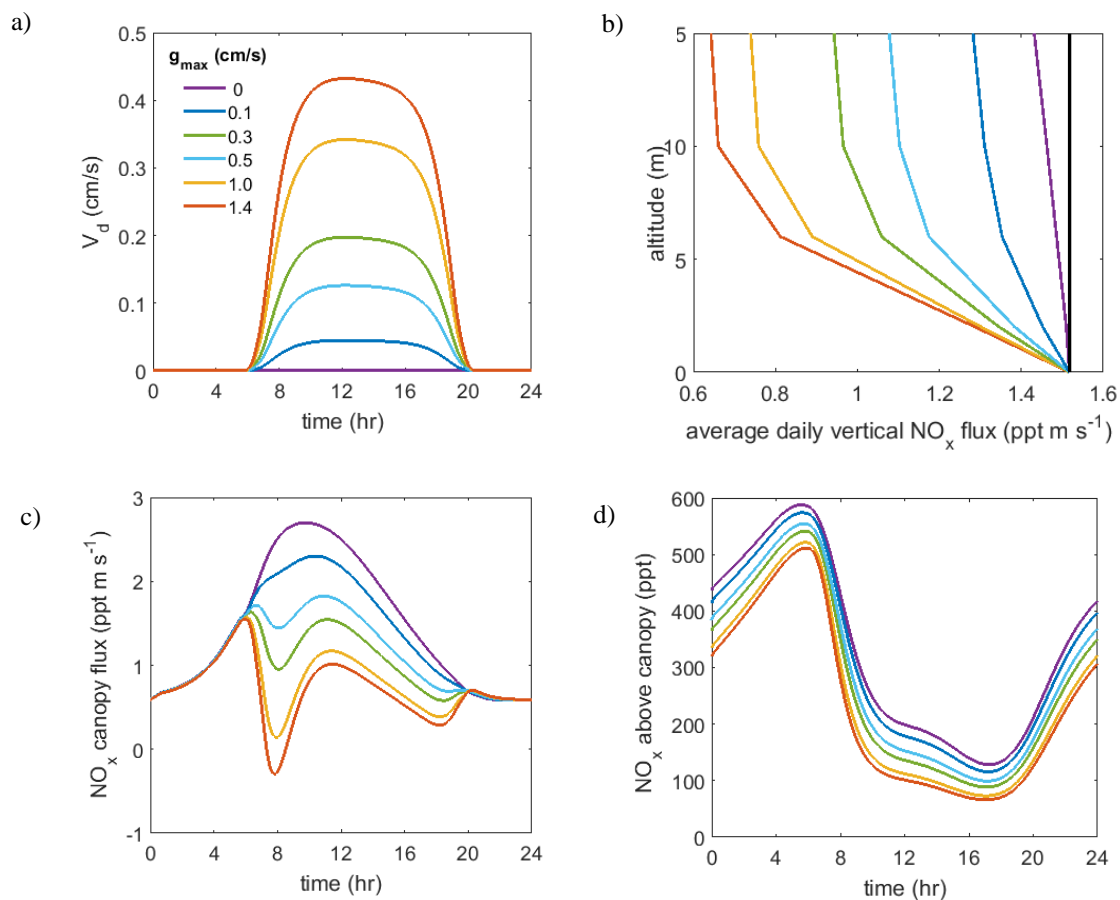
Figure 5: (a) Modeled diurnal NO₂ deposition velocities, (b) average daily vertical fluxes of NOₓ and a conserved tracer (black line), (c) diurnal canopy fluxes at 10 m, and (d) diurnal above-canopy NOₓ mixing ratios at 15 m for different values of g_{max} using the Wesely scheme to calculate stomatal conductance.
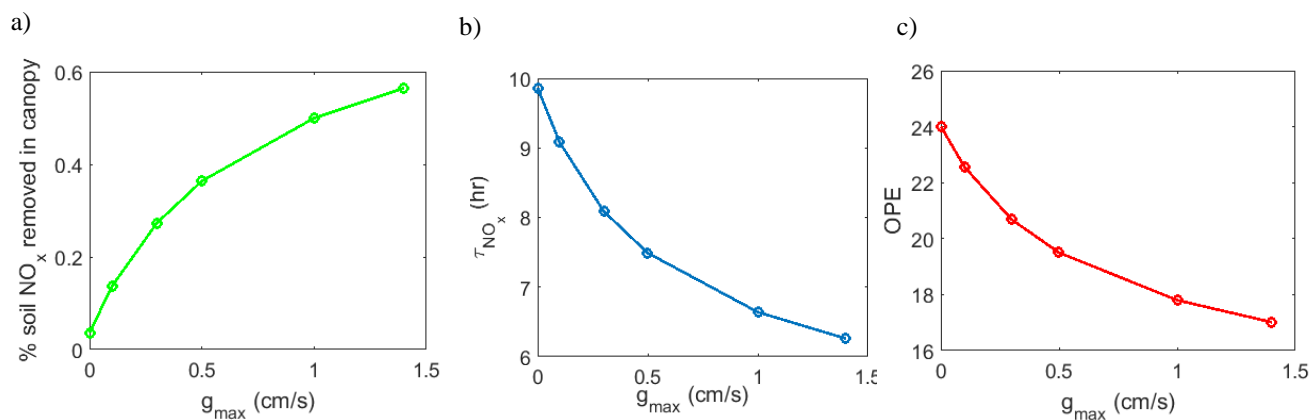
Figure 6: Model-predicted dependence of (a) the percent of soil-emitted NO$_x$ removed within the canopy, (b) the average daily NO$_x$ lifetime in the planetary boundary layer, and (c) ozone production efficiency (OPE) on g_{max} using the Wesely scheme to calculate stomatal conductance.
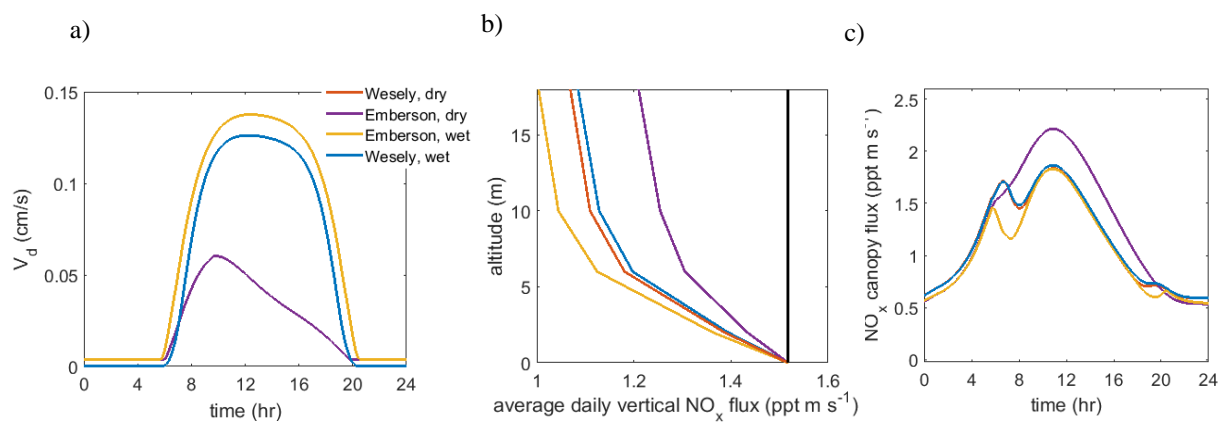
Figure 7: (a) Modeled diurnal NO₂ deposition velocities, (b) average daily vertical fluxes compared to a conserved tracer (black line), and (c) diurnal canopy fluxes at 10 m for "wet" and "dry" scenarios using either the Wesely or Emberson models to calculate stomatal conductance.
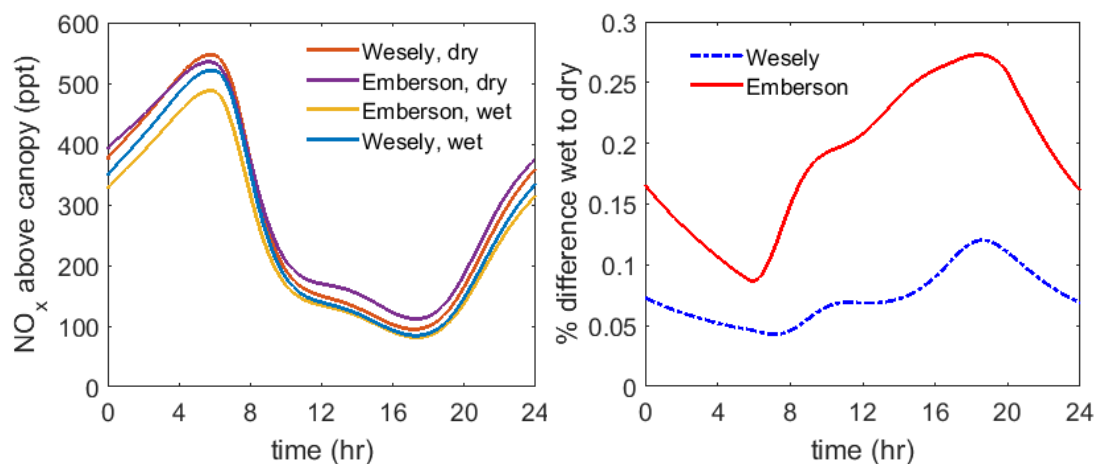
Figure 8: (left) Modeled NOₓ mixing ratios above the canopy at 15 m for "wet" and "dry" scenarios using either the Wesely or Emberson models to calculate stomatal conductance. (right) Percent difference between NOₓ mixing ratios on "wet" and "dry" days using either the Wesely (blue dashed line) or Emberson (red solid line) parameterization of stomatal conductance.
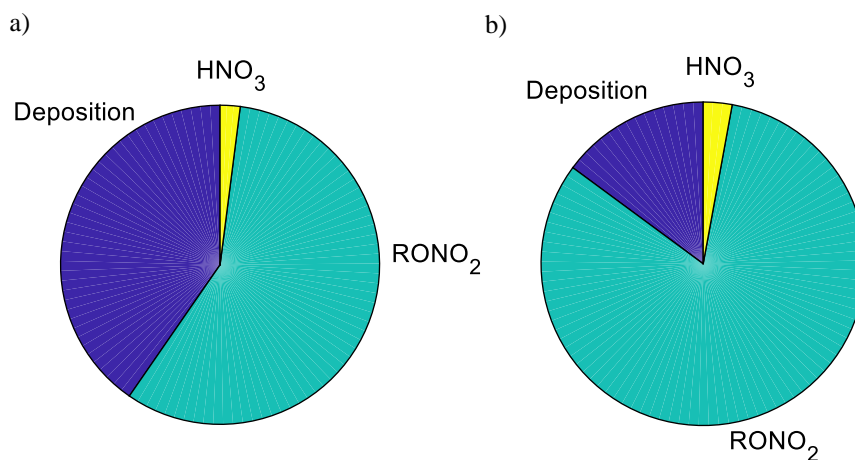
Figure 9: Model prediction for the fraction of NO$_x$ removed by deposition, nitric acid formation, and alkyl nitrate formation using the Emberson parameterization of stomatal conductance for (a) "wet" and (b) "dry" conditions.
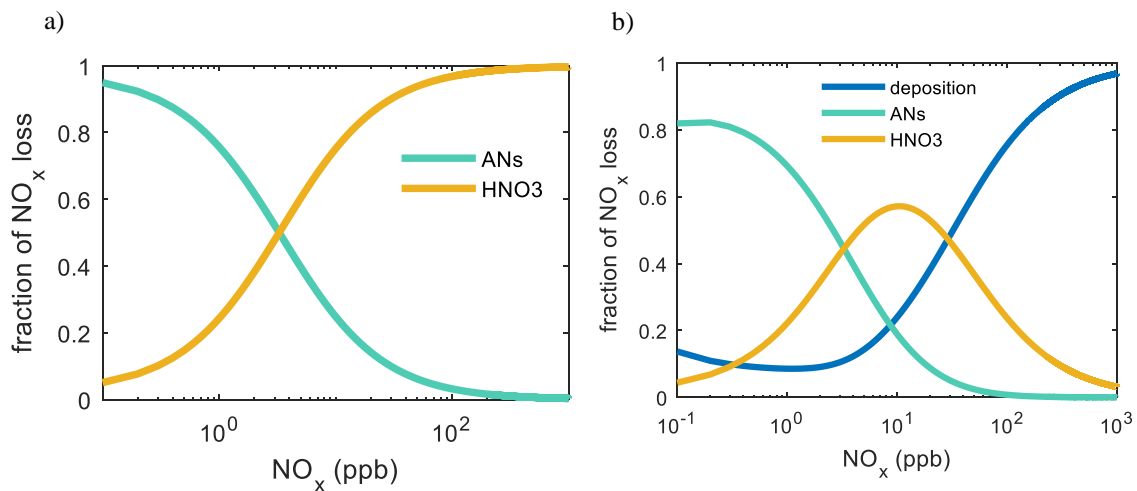
Figure 10: Fraction of NO$_x$ loss to alkyl nitrate formation, nitric acid formation with (a) no foliar uptake and (b) with foliar deposition as a function of NO$_x$ mixing ratio predicted by the simplified single-box model.